Modelling negative capacitance in bacterial biofilms, as seen in neurons

Livvy Hancock*, experiment performed in collaboration with Alice Gane under the supervision of Thomas Waigh based on work from Emmanuel U. Akabuogu and Victor Carneiro Da Cunha Martorelli.[1]
Department of Physics, University of Manchester, Greater Manchester, M13 9PL

(*Electronic mail: olivia.hancock@student.manchester.ac.uk)

(Dated: 7 January 2024)

Neuronal models were fit to Electrical Impedance Spectroscopy (EIS) data from bacterial biofilms exhibiting negative capacitance. The bacteria studied were *Pseudomonas aeruginosa* and two strains of *Escherichia coli*: DH5α and DH5α Δkch. The equivalent circuits were based on memristor and Hodgkin-Huxley models; we show that models developed for neurons can be applied to biofilms. A randles cell with a constant phase element (CPE) was found to best represent the electrode effects. We performed fits using Gamry software and then developed our own procedure using python code. We trialled different fitting routines including gradient descent, Nelder-Mead and Curve-fit listed in order of ascending success. Our code improves on Gamry fits but requires initial parameter inputs from Gamry so cannot fit from scratch. We also developed a code that fits from scratch but requires manual parameter adjustment so cannot be generalised to new EIS data. The Hodgkin-Huxley model with a CPE most accurately captured the internal dynamics of the biofilm. Negative resistances or negative inductances were found in both DH5α and DH5α Δkch strains of E. coli suggesting the presence of a sodium ion channel. We show that because the Hodgkin-Huxley model is based on physiological structures in the neuron, the equivalent circuit has redundant parameters. This means many equivalent fits can be found for a model with large variation in parameter values so drawing physiological conclusions from the optimised parameters may be erroneous. To conclude, a method was developed to study the composition and ion channels in biofilms which is of interest to global health[1] but care must be taken drawing conclusions from over parameterised model fits.

I. INTRODUCTION

A community of bacteria attached to a surface is known as a biofilm; they often secrete extracellular polymeric substance (EPS). EPS provides structural support, protects the biofilm from antibiotics and enables the transfer of nutrients and signals[2]. Forming a biofilm therefore provides a survival advantages to bacteria, including 500 times the antibiotic resistance[3]. In 2019 the World Health Organisation declared antimicrobial resistance as one of the top 10 threats to global health[4] and biofilms are implicated in over 65 % of bacterial infections[5]. *Escherichia coli* (*E. coli*) causes conditions such as diarrhea and urinary tract infections. It is also responsible for deaths from infection of medical devices such as prosthetic joints, grafts and catheters[6]. *Pseudomonas aeruginosa* infections have a 50 percent mortality rate in patients with cancer, cystic fibrosis, and burns[7]. It is therefore of great significance to global health to understand the internal dynamics of biofilms. Analysing the impedance spectra of biofilms to find accurate equivalent circuit models allows characterisation of biofilms. Physical equivalents can be hypothesised for the circuit elements and parameter estimates of resistance, capacitance and inductance provide information on the how the biofilm functions. It is thus possible to model how biofilms respond to stimuli to gain knowledge of how best to use antibiotics against them. The study of biofilm electrophysiology therefore has therapeutic applications in treatment of medical equipment and disease.

Equivalent circuit models have been used to study EIS spectra in neurons but not extensively in bacteria so this report aims to find whether the models are applicable to bacterial biofilms.

II. THEORY

A. Electrical impedance spectroscopy

EIS is a technique to measure the intrinsic material properties of a substance. An input sinusoidal voltage probes the biofilm and the sinusoidal current response is recorded for a range of frequencies. To do this an electrochemical cell is used, consisting of three electrodes: a working electrode (WE), upon which the biofilm was grown, a reference electrode (RE) and a counter electrode (CE). These are connected to a potentiostat and an electrolyte solution as shown in figure 1. A potentiostat is a device that controls the voltage difference (V) between the WE and RE. It does this by using an amplifier to monitor the V and augmenting the current through the CE accordingly to maintain the desired V[8]. In this experiment the WE was made of indium tin oxide, the RE of silver/silver chloride and the CE of platinum. The potentiostat used was a Gamry potentiostat so that it could be easily integrated with the Gamry software for analysing the spectra.

Impedance is a time varying equivalent of resistance so the impedence of the biofilm encodes information about all sources of opposition to current flow in the biofilm. During EIS the impedance of system is recorded across a range of frequencies, hence why it is termed spectroscopy. The beauty of EIS is that it leverages the fact that electrochemical events, such as a capacitor charging, occur on different timescales so recording the impedance for a range of frequencies allows emergent electrochemical phenomena to be displayed. Identification and classification of different features in the spectra gives insight into the physiological makeup of the the

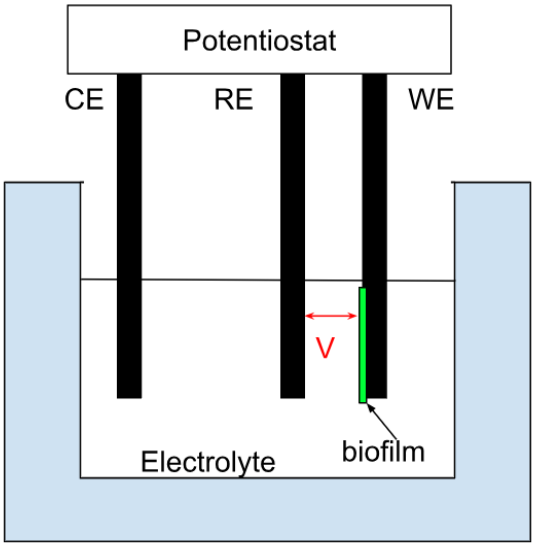

FIG. 1. The setup of the electrochemical cell for EIS. The working electrode (WE), reference electrode (RE) and counter electrode (CE) are shown in black. All electrodes are immersed in the electrolyte. The AC voltage applied across the RE and WE is shown in red. The biofilm bieng studied is green on the WE.

sample being studied.

The impedance for a given frequency, ω, is found by applying an alternating current (AC) voltage across the WE and RE: $V = V_0 \sin(\omega t)$ and measuring the current response of the biofilm sample on the WE $I = I_0 \sin(\omega t + \phi)$. ϕ is the phase difference introduced by the sample and V_0 and I_0 are the AC voltage and current amplitudes respectively. Generally, EIS phenomena are non-linear however if the voltage changes are small enough, they can be approximated as linear. V_0 must therefore be small (1 to 10 mV)[9] for the linear approximation to be valid, it was 10 mV for the data used in this report. An offset known as DC bias voltage can be added to the input voltage, changing the 0 amplitude position of the sine wave. The impedance is then calculated using

$$Z = \frac{V}{I}. \tag{1}$$

The input voltage and current response can be converted to exponentials using Eulers relation, so substituting V and I into the above relation yields the expression:

$$Z = Z_0 e^{i\phi} \tag{2}$$

for impedance[9]. This demonstrates how impedance spectroscopy reveals information about how a biofilm reacts to small ac voltage perturbations at different frequencies. The spectra can be modelled with different equivalent circuit elements that have different relationships of impedance and frequency. The impedance of a resistor of resistance R is $Z = R$

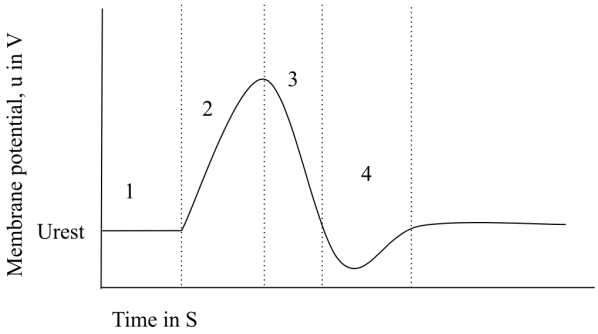

FIG. 2. A diagram of how the membrane potential progresses with time during an action potential.

as resistors do not introduce phase shift. A capacitor of capacitance, C, has impedance:

$$Z = \frac{1}{i\omega C}. \tag{3}$$

and an inductor of inductance L has impedance:

$$Z = i\omega L. \tag{4}$$

The Nyquist plot is a way to represent EIS data by plotting the imaginary part of the impedence on the Y-axis agains the real part on the X-axis. This type of plot is advantageous for viewing features of the spectrum such as negative capacitance which will be addressed in the following section. but lacks clear information about the impedance frequency relation. A Bode plot would be preferable to see how impedance varies with frequency as Bode plots have the phase angle and magnitude of the impedance plotted as different lines on the Y-axis against frequency on the X-axis. Nyquist plots will be used in this report when evaluating different models and fits as the feature of interest is the negative capacitance.

The Gamry software can be used to analyse the spectra obtained from the potentiostat. Equivalent circuit models can be created on Gamry and then fit with a Gamry autofit to the data collected. Gamrys autofit employs Nelder-Mead and Levenberg-Marquardt methods.

B. Negative capacitance

The feature of the impedance spectroscopy of particular interest in this report is negative capacitance as this is what introduces spiking behaviour[10]. An example of how negative capacitance manifests graphically is shown on figure 3. The low frequency loops seen for some DC bias voltages where the negative of imaginary impedance crosses the X-axis into the 4th quadrant of the graph is a feature associated with negative capacitance, inductance or negative resistance. Capacitance is the ability of a component to store charge, Q,

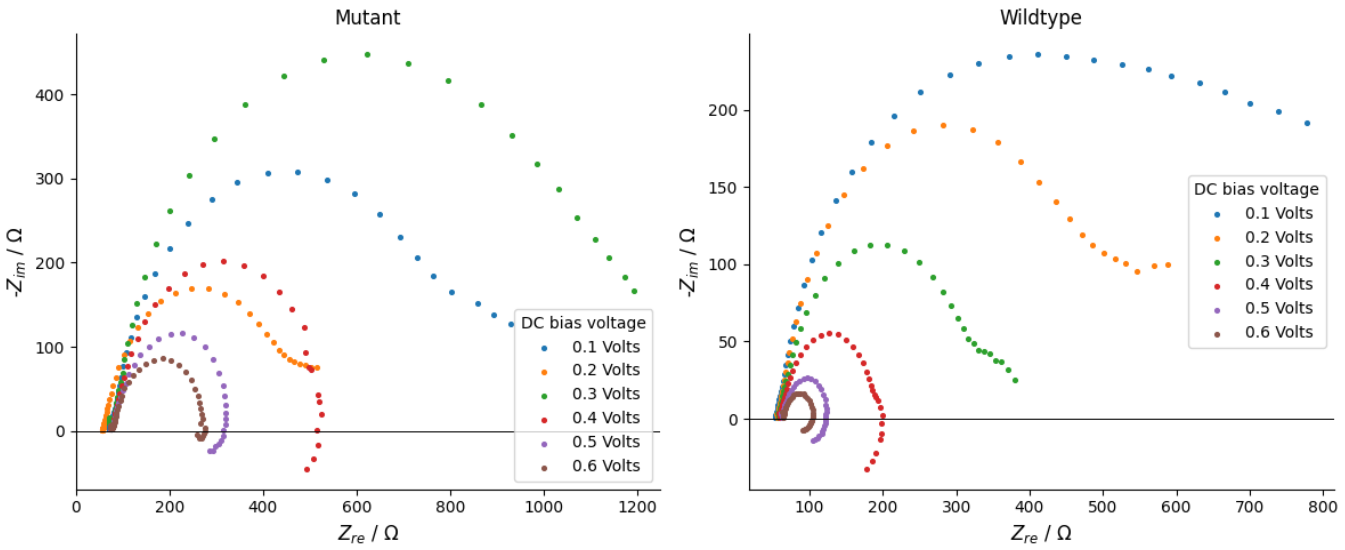

FIG. 3. The EIS spectra for *E. coli* for DC bias voltages from 0.1 to 0.6 V. The spectra for the mutant bacteria with no *kch* ion channel is shown on the left and the wildtype on the right. Both strains demonstrate negative capacitance for DC bias voltages of 0.4 V and above.

so can be found from the ratio of charge to applied voltage: $C = \frac{Q}{V}$. Negative capacitance indicates that charge stored decreases as voltage is applied which indicates the system must have agency over how voltage affects charge. Negative capacitance in biological systems could therefore be seen to be an implication of a living system[11]. It has been seen in neurons[12], pervoskite solar cells[13] and now in biofilms[14]. The physical causes of the negative capacitance phenomena will be subsequently discussed, though it remains a controversial topic in some materials such as pervoskite solar cells.

The first time negative capacitance was witnessed in a biological material was by Kenneth Cole in 1941. Cole developed a pioneering technique called voltage clamping that allowed the effect of voltage applied to a membrane on the flow of current across the membrane to be studied[15]. Cole took the axon of a giant squid as it was 1mm in diameter and applied two electrodes and an amplifier. He found negative capacitance which he called inductive reactance which he found 'shocking to the point of being unbelievable'[16].

Cole tentatively suggested that the negative capacitance was related to spiking behaviour and this was confirmed and modelled by Hodgkin and Huxley 1952[17]. They went on to find the role of voltage gated ion channels in producing action potential, developing a neuronal model for negative capacitance and spiking behaviour.

C. The Hodgkin-Huxley model

The Hodgkin-Huxley model provides a mathematical description of how current propagates through a membrane. Based on splitting the ionic current between two ion channels: sodium and potassium, with another channel for smaller leak

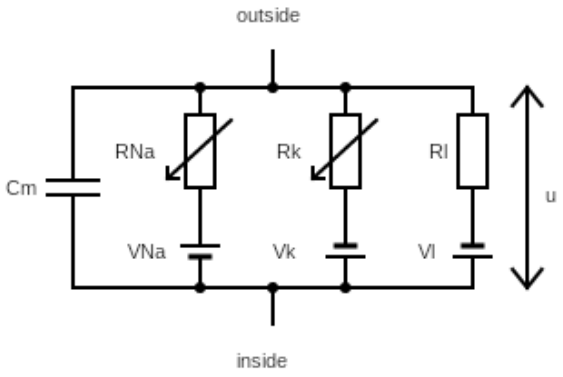

FIG. 4. The circuit for Hodgkin-Huxley model for a neuron. In a biofilm, in this the report the Na channel is replaced by a channel that represents the collective action of all channels other than potassium. The Rk channel and leak channel remain the same for the biofilm model as for the neuron model.

currents carried by chloride and other ions. Using a voltage clamp on a giant squid nerve fibre, they were able to measure conductances of the ion channels in relation to voltage and time. This was done by controlling ion concentrations in the extracellular fluid. They devised an equivalent circuit model shown in figure 4 where all components are modelling the inside of the cell membrane of a neuron. The labels inside and outside refer to the outside of the neuron and the inside of the neuron, thus the capacitor C_m is the membrane capacitance. u is the membrane potential, measured as the voltage difference between inside and outside the neuron. Each parallel branch then represents a different ion channel: R_{Na} represents the

resistance of the sodium ion channel which is time variable, as resistance is inversely proportional to conductivity which depends on the state of the ion channel[18]. E_{Na} represents the Nernst potential which is potential difference between the two sides of the ion channel at equilibrium due to the difference in ion concentration in and out of the cell[19].

Hodgkin and Huxley began with an expression of Kirchoff's Law:

$$I = I_c + I_K + I_{Na} + I_l \tag{5}$$

where I_K and I_{Na} are the currents through the potassium and sodium channels respectively, I_l is the leak current and I_c is the current through the capacitor. The summation of the branches of the equivalent circuit is equal to the input current, I as seen on figure 4. A capacitor is defined by the ratio of the charge on each plate, q, to the voltage between them. Here the voltage refers to the membrane potential: u. This can be rearranged for q and then differentiated to find

$$I_c = C\frac{du}{dt}. \tag{6}$$

The leak, sodium and potassium currents can be expressed in terms of their respective conductances, g_l, g_{Na}, g_K, using Ohms law and the principle that conductance is the inverse of resistance. Equation 13 can thus be reformulated:

$$C\frac{du}{dt} = I - g_K(u - E_K) - g_{Na}(u - E_{Na}) - g_l(u - E_l). \tag{7}$$

Here, the rate of change of voltage is expressed in terms of conductances of the different ion channels. This describes the dynamics of the action potential. Hodgkin and Huxley experimentally determined the parameters in the equation, paving the way for a physiological understanding of how the gating of different ion channels contribute to the stages of the action potential. Action potential is the mechanism for signal transmission within and across neurons. A series of action potentials is known as a spike train.

Membrane potential can be modified by opening and closing voltage gated ion channels. This allows the flow of ions in and out of the neuron which is the basis of electrochemical signalling. It follows a specific form known as the action potential, shown in figure 2. The behaviour of different ion channels to achieve the action potential is described subsequently. The resting potential, u_r, of a cell is the membrane potential in the absence of any input, shown in section 1 of figure 2. A neuron will then receive input, for example a neurotransmitter binding to a receptor and depolarisation will occur: stage 2 of figure 2. The membrane potential becomes less negative due to an influx of positive ions such as Sodium (Na^+). A positive feedback loop is established as more Na^+ ion channels open with the increasing voltage. This occurs until a critical voltage at which the Na^+ channels close and Potassium (K^+) open to allow efflux of K^+ out of the cell giving rise to an overall decrease in membrane potential. This is seen as stage 3 in figure 2: repolarisation. In stage 4 hyperpolarisation occurs whereby the efflux of positive ions gives rise to a membrane potential lower than the resting potential. This period of hyperpolarisation explains the refactory period of the neuron whereby it is almost impossible to trigger another action potential[19].

Hodgkin and Huxley found values for specific membrane capacitance (capacitance per are of membrane) of 0.8 and 1.5 μFcm^{-2} in Neurons. It has been shown more recently that these values may be over estimates due to roughness in the membrane and values of around 0.5 μFcm^{-2} have been put forward[20].

D. The bacteria

We performed our analysis on *E.coli* strains DH5α and DH5α Δ*kch*. DH5α is what is known as a wildtype as it has not been genetically altered. DH5α Δ*kch* is known as a knock down mutant as the potassium (*kch*) ion channel has been removed. This was done by P1 phage transduction which is a technique to modify bacterial genes. The *E.coli* biolfilms were grown on Indium tin oxide (ITO) electrodes with an area of 4 cm^2. Our analysis was extended to *Pseudomonas aeruginosa* (*P. aeruginosa*). The data on *E.coli* was produced by Emmanuel Akabuogu and the data on *P. aeruginosa* was produced by Adhvaidhi Kuntran, both of the Manchester Department of Physics Astronomy.

Bacterial ion channels have been studied with a patch clamp, a version of voltage clamping to study a single ion channel[21]. Amongst those found in *E. coli* are potassium (K^+), sodium (Na^+), calcium (Ca^{2+})[22] and chloride (Cl^-)[23]. Potassium ion channels have been implicated in electrical signalling to communicate stress: when a bacteria near the centre of the biofilm is deprived of nutrients it can communicate this metabolic stress by releasing potassium and hyperpolarizing. Surrounding cells take in the potassium and depolarise which causes them to take in fewer nutrients. A wave is created that enables more nutrients to reach the centre, increasing the survival chance of the bacteria at the centre and therefore the whole biofilm[24]. Potassium ion channels are therefore a key factor in bacterial communication and survival. The ion channels are voltage gated so EIS data provides a rich spectra to analyse the voltage behaviour of the ion channels. Modelling the EIS data has the potential to enhance our knowledge of the dynamics of the ion channels.

III. THEORY OF FITTING ROUTINES

The project hinged on fitting models to data so understanding the fitting routines was essential for choice of fit and dealing with fitting issues.

All fitting regimes find the parameters that minimise the difference between data and a model. This difference will be referred to as the loss function, L, and there are choices of how

this is defined. An example is the least squares loss function, defined as:

$$L = \sum_{i=1}^{n} (y_i - f(x_i, \theta))^2 \tag{8}$$

where n is the number of data points in the experimental data and $f(x_i)$ is the model function acting on the x values of the experimental data, in this case the x values are frequency. θ represents all the parameters of the model. The different fitting routines prescribe different algorithms to minimise L.

A. Gradient Descent

Gradient descent navigates the loss function to find a minimum by moving down the gradient in steps defined by the learning rate. Starting from a user defined initial point, the gradient of the loss function is calculated with respect to each parameter and the new parameters are updated proportional to the gradient and learning rate, η. In mathematical words this can be written:

$$\theta_{new} = \theta_{old} - \nabla_\theta \eta. \tag{9}$$

The algorithm then calculates the gradient at the new parameters, iteratively moving down the loss function until the parameter updates are small enough for convergence to be considered reached. It is an increasingly popular optimisation algorithm especially for neural networks; however straightforward gradient descent as described above has a number of issues which has lead to many variants of gradient descent to deal with these. Gradient descent struggles to navigate saddle points in parameter space as the gradients can become vanishingly small. This means updates are not large enough to escape the saddle point which can result in non convergence, a failure to fit. Another difficulty simple gradient descent faces is that the learning rate is constant across all parameters which may not be ideal as parameters may need to be updated at different rates as they have different effects on the data.[25].

B. Curve fit

Levenberg-Marquardt algorithm (LMA) addresses the issues experienced by gradient descent close to convergence by combining gradient descent with another algorithm: the Gauss Newton method. The Gauss Newton method approximates the loss function as quadratic to update the parameters. Combining the two approaches, the LMA calculates a damping factor at each iteration which controls the relative contributions of the Gauss Newton and gradient descent methods in updating the parameters such that it resembles GD far from the optimal parameters and Gauss Newton when near[26].

Curvefit is an inbuilt SciPy function that employs the LMA to minimise the loss function. The LMA begins with an initial guess of the parameters. Unless manually input, curvefit uses initial guesses of 1 for all parameters[27].

C. Nelder-Mead

The Nelder-Mead algorithm is unlike those previously discussed as it does not require calculations of gradients. Instead it uses a geometric simplex (the notion of a triangle generalised to higher dimensions, in this case the number of dimensions of the parameter space) in parameter space[28]. Updates are performed by calculating the values at each vertex of the simplex and rejecting that with the highest value so the triangle becomes iteratively closer to the minimum of the loss function. Near the minimum the simplex size reduces until it gets small enough to consider convergence achieved[29].

IV. METHODS

A. Code development

A code was developed to fit equivalent circuit models to data, outputting the parameter values of elements in the equivalent circuit that optimised the fit. The code is designed for EIS data, working with the real and imaginary values of impedance at each frequency. Firstly a function is defined for the desired equivalent circuit models. The function takes frequency and parameters used in the equivalent circuit model as arguments. It returns real and imaginary impedance based on the equation specific to the circuit. A fitting procedure then compares data produced by the model to the experimental data and optimises the model parameters.

B. Error calculation

The uncertainties on the parameter values were initially calculated using bootstrapping. It is a technique that allows errors to be calculated from empirical data without knowledge of the underlying distribution. This allows error estimation when the error on the empirical data is not known as was the case in this experiment. The bootstrapping algorithm involves drawing N independent samples from the empirical dataset. These are drawn with replacement so there is a high probability of repeated data points. Each of the N samples were used as data and put into the fit model to produce optimised parameter estimates. The standard deviation, σ, of the optimised parameter values across the N samples was calculated as the uncertainty:

$$\sigma = \sqrt{\frac{\sum (x_i - \mu)^2}{N}} \tag{10}$$

x_i refers to the optimised parameter for one of the N samples so the sum runs over $i = 0$ to $i = N$. μ is the mean over all N samples. This provides a measure of the spread of data about the mean which indicates the uncertainty in the fit parameter[30].

However, using the bootstrapping method gave uncertainties that generally increased with the number of samples

drawn, indicating it was not an accurate estimator of error. Error should be a property of the model fit not of the way the error is calculated. The increasing error with N was likely due to the fact that the fitting procedure could not converge to optimised parameters for some of the samples. Thus as a larger number of samples were drawn, the uncertainties calculated increased as there was more spread in optimised parameters.

It was therefore decided that extracting uncertainties from curvefit and plotting the residuals was a more accurate way to calculate uncertainties. The chi squared value was not used as it is not a valid way to quantify goodness of fit for non linear fits[31]. If the experiment were to be extended, a quantitative way of classifying the goodness of fit would be beneficial.

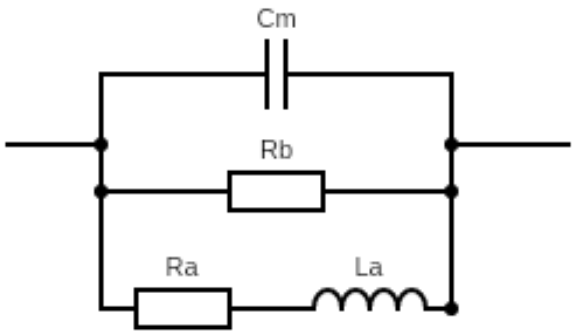

FIG. 5. Circuit a. An equivalent circuit for a memristor model created on Gamry. Components labelled R, C and L represent resistors, capacitors and inductors respectively.

V. MEMRISTOR MODEL

A memristor is a two terminal device proposed by Chua in 1971 as the missing 4th circuit element[32]. The novelty of the memristor lies in its ability to change its resistance based on previously applied voltage. This memory property makes it a tantalising prospect for neuromorphic computing as they can emulate synapses or neurons depending on how they are programmed[10]. Their memory properties also make them a suitable candidate for modelling negative capacitance. There are many configurations that could consitute a memristor, one of which is shown in figure 5. The capacitor is not always present in a typical memristor but has been included as EIS data often represents charge storage phenomena so a capacitor is an appropriate circuit element for models. A 2021 article by Bisquert suggested that memristor models could be used to model negative capacitance in neurons so we attempt to extend the method to bacteria. We used the memristor model as a preliminary model. We fit the memristor model to the mutant data as it had the potassium ion channel removed so we thought it could be described by a more basic equivalent circuit as there are fewer ion channels to model. Perhaps this was a simplification as there are not simply two bacterial ion channels; we are modelling the collective action of all ion channels that are not potassium with one branch of the equivalent circuit.

To investigate how accurately a memristor could represent the internal dynamics of the biofilm the equation governing the impedance in a memristor was calculated. This was done using the relations between circuit elements and impedance and the rules for adding series and parallel resistances[33]. The impedance was found to be:

$$Z = (i\omega C_m + \frac{1}{R_b} + \frac{1}{R_a + i\omega L_a})^{-1}. \tag{11}$$

We attempted to fit the memristor model shown in figure 5 to *E.coli* data for a range of bias voltages using the Gamry software but it did not converge to a fit. This indicated that the memristor was a poor descriptor of the biofilm. We did however persist, getting the Python code to fit the model using the Nelder-Mead method. The results for 0.5 DC bias voltage are shown by the purple line on figure 7. The model did not provide a good fit to the data, suggesting the physiology of the biofilm is not well described by the a memristor model. The memristor did, however model the negative inductance loop where the imaginary impedance crosses the real axis confirming that the memristor circuit can model negative capacitance effects. There seems to be an offset in the fit which we will later see is likely due to effects at the electrode. The optimised parameters are not stated as they are irrelevant given they do not fit the data. Instead of trying to improve the fitting regime, we trialled different models as if the model does not capture the data it is not useful to try to improve the fit.

VI. HODGKIN-HUXLEY MODEL FOR MUTANT E.COLI

A. Method and results without a CPE

The Hodgkin-Huxley model can be used to describe *E. coli* strain DH5α Δkch by representing the collective action of all ion channels other than the potassium with one branch of the Hodgkin-Huxley circuit. The circuit used is shown in figure 6. The top branch contains a Capacitor C_m that models the membrane capacitance as usual. The next two branches down containing inductor L_n resistor R_n and resistor R_q model the action of the voltage gated ion channel. They are equivalent to one branch of the Hodgkin-Huxley circuit of figure 4 with a battery and variable resistor. This substitution is made because the battery and variable resistor branch has time dependence that complicates the analysis of the impedance response of the circuit. Fortunately, the small amplitude approximation can be made as the AC voltages used in EIS are low (10 mV in this experiment). By assuming that for small signals the variable resistor has minor variations about a fixed point it can be modelled by resistors whilst an inductor models the energy

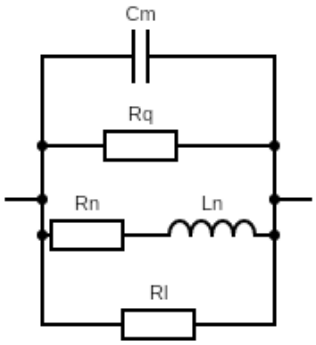

FIG. 6. An equivalent circuit for the Hodgkin-Huxley model with a single channel representing collective action of many ion channels.

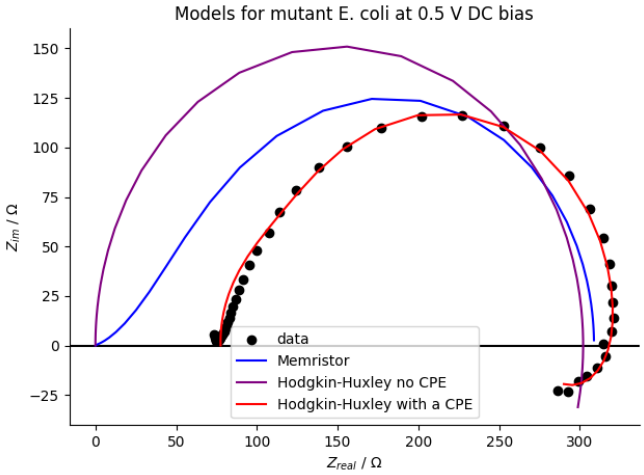

FIG. 7. This figure shows a comparison of the memristor model and Hodgkin-Huxley model with and without a CPE for the data from the DH5α Δkch strain at a DC bias voltage of 0.5V. All models were fit with the Nelder-Mead method.

storage aspect. The lowest branch seen on figure 6 with resistor R_l corresponds to the smaller leak currents carried by ions such as chloride. The small amplitude approximation allowed for the derivation of the impedance for the single channel Hodgkin-Huxley model:

$$Z = (i\omega C_m + \frac{1}{R_q} + \frac{1}{R_n + i\omega L_n} + \frac{1}{R_l})^{-1} \tag{12}$$

The model was fit using the Nelder-Mead algorithm on Python and it is shown by the purple line in figure 7 that this was not a successful fit to the data. There appears to be a systematic error. To rectify this, the effects at the electrode are considered.

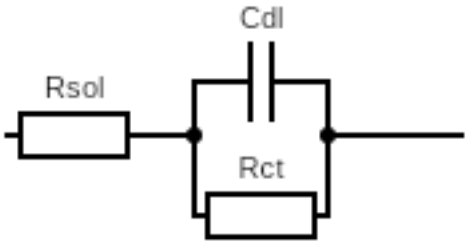

FIG. 8. The circuit diagram for a Randles cell which attempts to capture ionic behaviour at the electrode during EIS. R_{sol} denotes the solution resistance and R_{ct} characterizes the resistance linked to Faradaic current. C_{dl} models the double layer capacitance, representing the capacitive effects at the electrode-solution interface.

B. The need for the CPE

During electrical impedance spectroscopy positive charges in the solution are attracted to the negative electrode and vice versa. Opposite charges build up in the solution and electrode, separated by a region called the electrical double layer (EDL) which acts as a dielectric forming a capacitor known as a double layer capacitor. It is known that the EDL is caused by a build up of counter ions that maintain neutrality on the electrode surface, but modelling the EDL is an active area of research[34].

There is a current associated with the double layer capacitance, known as a non-Faradaic current as no charged particles are passing between the solution and the electrode to carry the current. There is also Faradaic current due to charged particles moving from the electrolyte to the surface of the electrode in reduction and oxidation reactions. It is termed Faradaic as it complies with Faradays laws. For an ideal electrode only Faradaic current would be experienced but in real electrodes both currents are present. The two effects give rise to features in impedance spectra so must be accounted for in the equivalent circuit while appreciating they are features of the data collection method rather than the biofilm itself. The EDL giving rise to non-Faradaic current is modelled as a capacitor, C_{dl} where dl stands for double layer. The Faradaic current can be seen as a leak current which is an additional way for current to flow to the electrode and is thus modelled as a resistor, R_{ct}, added in parallel with the capacitor as shown in figure 8. The ct in R_{ct} stands for charge transfer as there is movement of charged particles producing the Faradaic current. Finally to account for the resistance of the solution, another resistor, R_{sol}, is added to the equivalent circuit in series with both the capacitor and resistor R_{ct} as current must pass through the solution before reaching the electrode[35]. These components make up what is known as the simplified Randles cell[33] which is shown in figure 8.

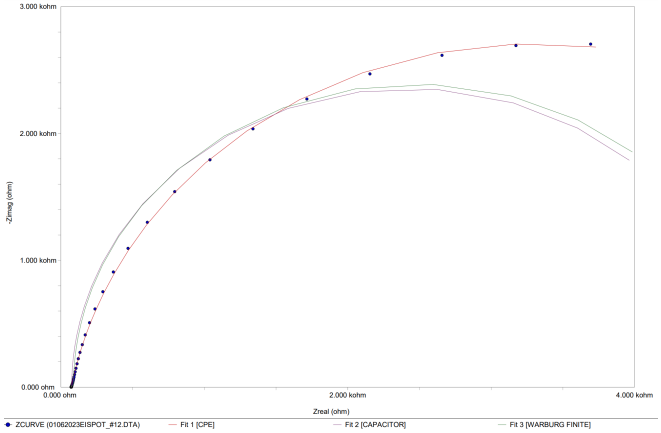

FIG. 9. A screenshot from Gamry software showing a plot of the data points for the biofilm at 0V dc bias, fitted with a capacitor in purple, the finite Warburg element in green and the CPE element in red. The CPE element provides a much better fit to the data than a Warburg element or capacitor.

We attempted fits with different arrangements of the Randles circuit that provided equally good models to fit the data. The resistors R_{ct} and R_{sol} can be put in series with one another and in parallel to C_{dl} which fit the data slightly better. This highlights the finding that there are many equivalent circuits that can be used to model the data so arrangements should be selected on a physiological basis. We therefore chose the model to pursue on a physiological basis to make the results more applicable to the biofilm.

To test what arrangement of circuit elements best captured the electrode behaviour, different models were fit to the DH5α Δkch data with 0 V bias voltage. The rationale behind this was the idea that the ion channels are voltage gated and so perhaps require a DC bias to become active. We thought that at 0 V we would effectively be modelling just the electrode effects. Whilst this method worked to find an effective way to model electrode effects, more research would be required to state with certainty how the DC bias voltage affects the spectra. The purple line on figure 9 shows the fit of the Randles cell to the data. The poor fit demonstrates that the circuit does not capture the behaviour at the electrode and other models must be considered.

The fit is rectified by modelling the capacitor as a non-ideal capacitor that undergoes capacitance dispersion. This is the constant phase element, which has been being referred to as the CPE, which manifests mathematically by modifying the impedance to incorporate a power law. The impedance for the double layer capacitor is:

$$Z = \frac{1}{i\omega C_{dl}}. \tag{13}$$

The impedance of the CPE component is:

$$Z = \frac{1}{(i\omega)^{\phi} T}, \tag{14}$$

where ϕ is the CPE exponent which is between 0 and 1[36]. T is the double layer capacitance parameter in $\mathrm{Fcm^{-2}s^{-1}}$. As ϕ tends to 1, ideal capacitor impedance is recovered and if $\phi = 0$ the impedance becomes independent of frequency as can be seen from the equations above. The infinite Warburg element is a specific case of the CPE where $\phi = 0.5$ and is used when the diffusion path is infinite. This is not the case for charge transfer at the electrode so the finite Warburg was used. The fit for the finite Warburg element is shown in green on figure 9 and has impedance

$$Z = \frac{1}{(i\omega)^{\phi} T} \tanh(B(i\omega)^{0.5}). \tag{15}$$

Here, B is another fit parameter relating to the diffusion coefficient the thickness of the diffusion layer. The impedance of a capacitor is purely imaginary but a CPE has imaginary and real impedance, the real part is resistive, representing the non ideal dispersive nature of the non ideal capacitor[37]. Whilst addition of the CPE improves the success of the power of the model to fit the data it is difficult to describe its physical significance rendering its presence controversial[38]. ϕ has been shown to represent surface roughness[39] but has also been shown to be related to features of the porus electrode[36]. In summary, the CPE represents the imperfect double layer capacitance but exact physiological counterparts for the elements is still a topic of research.

The Randles circuit with the capacitor replaced by a CPE component with impedance written in equation 15 is shown as the red line on figure 9. It can be seen that the CPE equivalent circuit with ϕ and T as fit parameters of the model was more successful than the Warburg or ideal capacitor models. The CPE element was thus chosen over the Warburg or capacitor for subsequent models, using ϕ and T as parameters to be optimised.

C. Hodgkin-Huxley model with CPE

Equation 12 was modified to include the constant phase element:

$$Z = R_{sol} + (\frac{1}{R_{ct}} + (i\omega)^{\phi} T)^{-1} + (\frac{1}{R_q} + \frac{1}{R_n + i\omega L_n} + \frac{1}{R_l} + \frac{1}{\frac{1}{R_{ct}} + (i\omega)^{\phi} T})^{-1}. \tag{16}$$

This improved the fit which is shown on figure 12 for all DC biases. Our code consistently provided fits that seem more representative of the experimental data than the Gamry fits. This is most obvious for the 0.5 V DC vias voltage where the

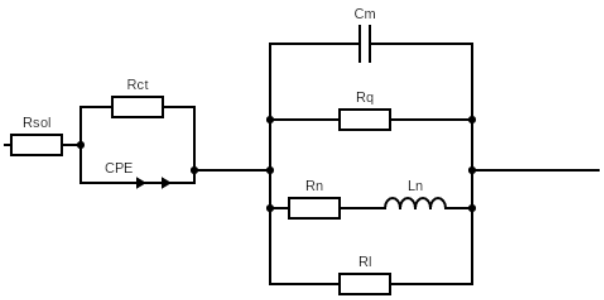

FIG. 10. Circuit b. An equivalent for the Hodgkin-Huxley model for a single channel, including a CPE.

Gamry fit does not enter the 4th quadrant and therefore does not represent the phenomena of interest. Neither our code using Gamry initial values nor the Gamry code successfully fit the low frequency negative inductance loop for DC biases of 0.4 or 0.7. This suggests a fault with the data, model or the fitting procedure. To test whether the fault was in the fitting procedure, we hypothesized that the number of parameters was too great for the fits to optimise efficiently and they may be getting trapped in local minima in the loss function due to the difficulty of navigating a high dimensional parameter space. This prediction was confirmed when we kept the parameters of the CPE (R_{sol}, R_{ct}, T and ϕ) and capacitance (C_m) constant leaving only the parameters associated with the leak current and ion channel (R_l, R_q, R_n and L_n) to vary. We obtained fits that entered the 4th quadrant as they necessary to encapsulate the data. The initial parameters used were: $R_{sol} = -1.6 \times 10^2$, $R_{ct} = -1$, $T = 1$ and $\phi = 3.5 \times 10^{-5}$ and $C_m = 5.5 \times 10^{-5}$. They were selected as the best parameters from multiple randomly initialised Nelder-Mead fits. We were thus able to capture negative impedance where Gamry could not, using no initial parameters from Gamry. The fits for 0.4, 0.5 and 0.6 V are shown on figure 11. All plots are displayed as Nyquist plots as while Bode plots may give a clearer depiction of the frequency dependence of the fit it does not display information about how well the fit captures the negative capacitance behaviour that is central to the investigation. This code can be provided on request via the email listed. This procedure performed with Nelder-Mead, Gradient descent and Curvefit all of which yielded similar results. This method would be reproducible for other bacteria with physiology that can be represented by circuit b. The conclusion can be drawn that when fitting routines are not converging to a fit, it may not indicate fault with the model but perhaps that too many parameters make convergence difficult.

The parameters extracted for the ion channel branch for 0.4, 0.5 and 0.6 V bias voltages are shown in table I. The table shows a comparison of the parameters stated in Akabuogu's article and those obtained by our code described above that optimised only 4 parameters. There is an additional line in the table with the parameters obtained from our fit where all 9 parameters in circuit b were optimised. This is the only fit from which a negative R_n value was obtained. This could be because the 4 parameter fit had negative values already set into the parameter definitions of the solution resistance and charge transfer resistance and therefore negative R_n values were not necessary to represent the impedance loop in the data. It is an interesting result that similar fits, which both capture the impedance data, can yield very different optimisation parameters. Before drawing conclusions about the physiology of the bacteria from the parameters, it must be appreciated that there are many sets of optimised parameters which fit the EIS data well.

There remains the question of why Gamry could not fit the data; perhaps the DC bias voltages other than 0.5 were causing artefacts in the data that meant there were phenomena in the data other than the expected behaviour of the biofilm. The model would then not accurately fit the data. To test whether there is an issue in the data a Kronig-Kramers transform can be used[40], this would be a good extension to add to our code. A more likely reason Gamry failed to accurately fit the negative capacitance is that the auto fit restricts the resistor values to positive.

VII. FITTING REGIMES

The Gamry 1 software gives different fit results when the components of the circuits are wired together differently, even if the circuits are equivalent under usual circuit rules whereby wires without a component are at the same potential. This suggests that the circuit modelling in Gamry has issues computing how nodes in the circuit affect the impedence equation.

Fitting the data without using Gamry was done to better understand the data and have control over the model and fitting procedures used. The Nelder-Mead and Gradient descent algorithms required initial parameter guesses to fit the models, introducing a choice of initial parameter values. One option was to use knowledge of their real physical equivalents, for example the capacitance of a cell. However, some of the physical equivalents of the model parameters, for example the resistors don't have well defined values in nature as they do not represent a specific physiological element of a biofilm. Instead, they model the action of a channel. Perhaps one could constrain the resistors to be positive but as discussed later this may not be necessary.This is reflected in the high variability of these values from the fits. The initial parameters guesses would therefore require a range too wide to produce satisfactory fits if they were based purely on knowledge physical equivalents of parameters.

A more effective approach used was to randomly initialise the initial parameters and replay the code until a suitable fit

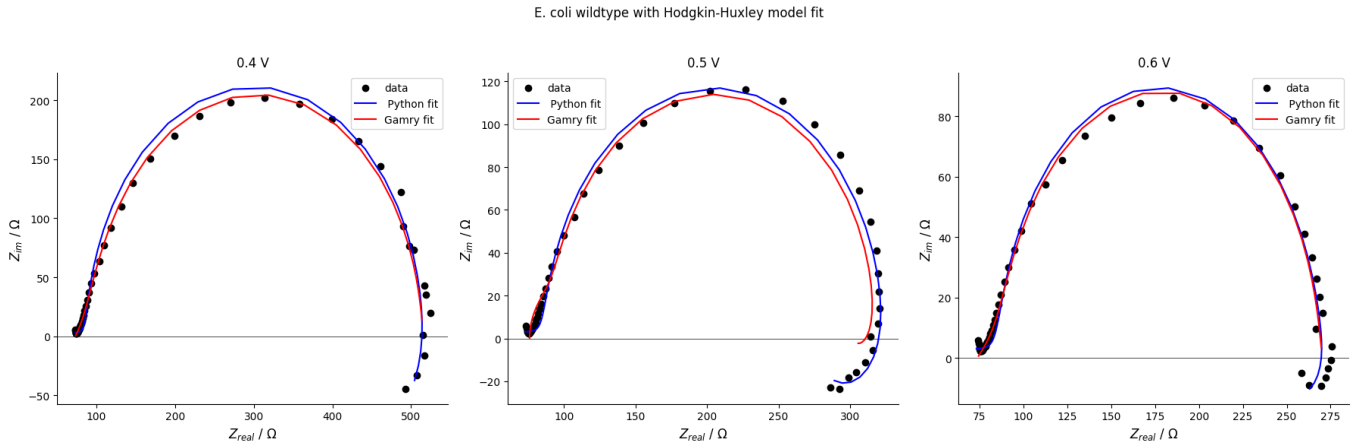

FIG. 11. Circuit b fit to DH5α Δ*kch* data using constant CPE parameters, with Gamry fit shown in red for comparison.

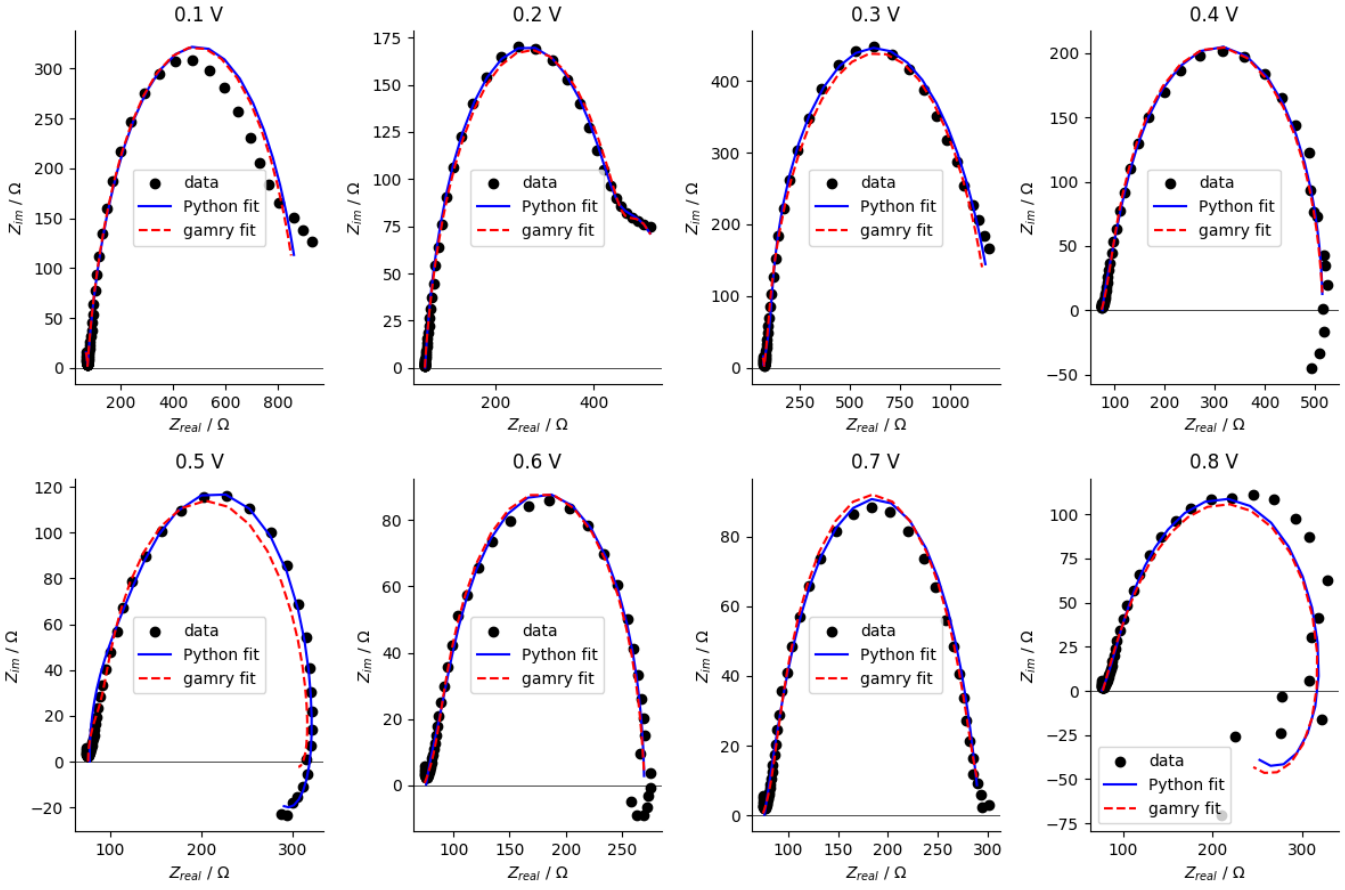

FIG. 12. The data for the DH5α Δ*kch* strain of *E. coli* is shown with the model fit obtained from Gamry shown in red. The fit performed with a Python code that optimised all parameters associated with the model using Gamry initial values is shown in blue. The model used was circuit b.

was produced. One could then tune the initial parameters from there. This enabled the fitting routines to be used with no prior knowledge from Gamry. A success of this approach was that it allowed for a deeper understanding of the parameters as through random initialisations, different parameters could be varied and their effects on the fit of the model could be studied. For example through this method it became clear that the CPE element controlled the positioning of the model curve but no amount of optimisation of the CPE could display negative capacitance, for that the other

TABLE I. This table shows the fit parameters for the DH5α Δkch so these parameters correspond to the combined action of ion channels other than potassium. The Python fit to all parameters is shown only for 0.5 V because that is the only fit that converged to display the negative capacitance.

DC bias / V	fit	R_l/Ω	R_n/Ω	L_n/H	τ_n/s
0.4	Python	$900 \pm 30 \times 10^7$	$700 \pm 10 \times 10^7$	500 ± 300	5 ± 3
	Akabuogu	429 ± 3	14800 ± 100	0.014 ± 0.001	$(94 \pm 7) \times 10^{-8}$
0.5	Python all parameters	16 ± 2	-11.1 ± 0.7	2.2 ± 0.6	-0.20 ± 0.05
	Python	$400 \pm 80 \times 10^6$	$500 \pm 10 \times 10^7$	700 ± 40	0.7 ± 0.05
	Akabuogu	1920 ± 20	25 ± 3	16 ± 2	0.6 ± 0.1
0.6	Python	$300 \pm 10 \times 10^7$	$400 \pm 10 \times 10^7$	700 ± 300	1.4 ± 0.6
	Akabuogu	1770 ± 10	260.8 ± 0.6	0.00090 ± 0.00005	$(34 \pm 2) \times 10^7$

parameters: R_q, R_n, L_n, R_l had to be optimised. A downfall of this approach is that it requires manual changing of initial parameters, which is not efficient for generalising the model to other data sets. The conclusion drawn from this method was the high variability of some parameters and how little effect they had on the model. Examples of this are shown in the discussion of the parameters.

The effectiveness of fitting regimes will be shown and dicussed for the 0.5 V bias data from the DH5α Δkch but similiar results were found across all bias voltages. Figure 13 shows a comparison of the fits obtained using the circuit b model with constant CPE values and randomly initialised parameters R_q, R_n, L_n, R_l. The resistors had a range of 10 to 1000 for random initialisations and the inductor had a range of 1000 to 2000. These ranges were iteratively selected by modifying the range and seeing the effect on the fits; manually determining which initial parameters resulted in convergence to good fits. Whilst a tedious exercise that could not be generalised to large data sets, it gave a good indication of what parameter values should be and how sensitive the fits were to each of them.

We found in general that gradient descent performed worse than NM and Curvefit which often yielded similar optimisations. In figure 13 it can be seen that gradient descent converges to a local not global minimum which was often the case. To avoid convergence to local minima stochastic gradient descent could be employed. Stochastic gradient descent involves randomly selecting a batch of data points for which to calculate the gradient instead of using the average gradient for all data points as vanilla gradient descent does. The random selection of data points adds noise which makes the algorithm less sensitive to the local shape of the cost function so it can escape local minima. We focused on curvefit and NM instead of improving the gradient descent algorithm as they seemed capable of fitting the data.

The curvefit algorithm given the same initial parameters managed to evade the local minima, outperforming gradient

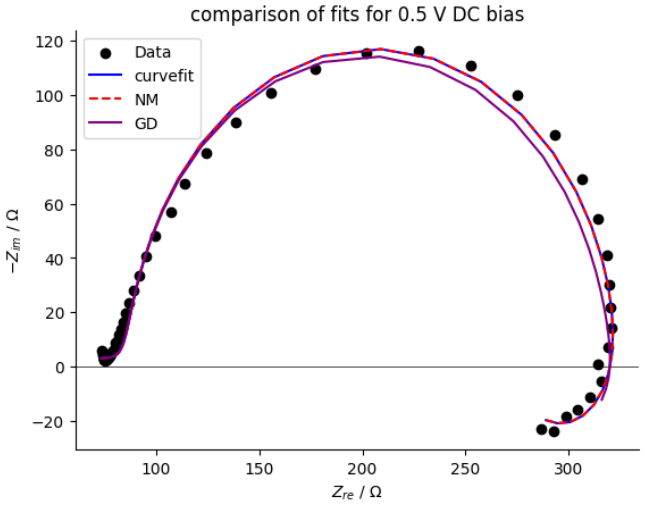

FIG. 13. A comparison of the Curvefit, Nelder-Mead and Gradient descent fit routines shown fitting the Hodgkin-Huxley model with a CPE to data from DH5α Δkch. This graph is one implementation of the different fits but because the parameters are randomly initialised the fits show variation each time the code is run.

descent algorithm. This makes sense given that the LM algorithm implemented by curvefit deals with otimisation near convergence using the Gauss Newton method, which is more appropriate than gradient descent when the gradients become small (near convergence).

The NM algorithm perfomed similiarly to curvefit overall, converging to almost visibly identical fits for 0.2, 0.4, 0.5, 0.6, 0.8 V with NM performing better for 0.1 V and 0.7 V but curvefit performing much better at 0.3 V.

We also found that even when routines converge to almost identical fits, parameter values can still show large variation. For example on figure 13 the NM and curvefits are not visibly distinguishable but for the parameter R_l they yield optimised parameters 346 Ω apart.

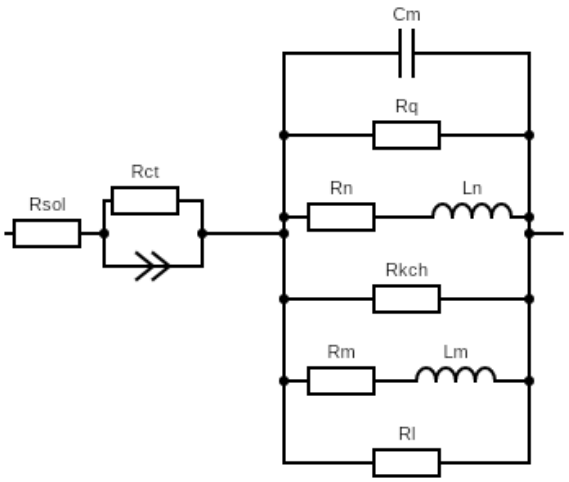

FIG. 14. Circuit c. An equivalent circuit from the Hodgkin-Huxley model created on Gamry. Components labelled R, C and L represent resistors, capacitors and inductors respectively.

VIII. HODGKIN-HUXLEY MODEL FOR WILDTYPE

Next, circuit c which is shown in figure 14 was fit to EIS data from the *E. coli* wildtype. The derivation of circuit C from the Hodgkin-Huxley neuron model shown in figure 4 is explained as follows. The components R_q, R_n and L_n represent the sodium branch with a variable resistor R_{Na} and battery V_{Na} under the small signal approximation as before in circuit b. In our model this configuration of components represents the combined action of many ion channels in the bacteria except potassium. This is a deviation from the Hodgkin-Huxley model where each branch represents one specific ion channel. The components labelled R_{kch}, R_m, L_m represent the potassium ion channel which is shown on the Hodgkin-Huxley circuit as a series variable resistor,R_k , and battery, V_k. R_l represents the final branch on the Hodgkin-Huxley model: the smaller ionic currents such as chloride as before. The equation calculated for the impedance of this circuit is as follows:

$$Z = R_{sol} + (\frac{1}{R_{ct}} + (i\omega)^{\phi} T)^{-1} + (i\omega C_m + \frac{1}{R_l} + \frac{1}{R_q} + \frac{1}{R_{Kch}} + \frac{1}{R_n + i\omega L_n} + \frac{1}{R_m + i\omega L_m})^{-1}. \quad (17)$$

We modified the functions of the circuit used in our code to account for the extra ion channel in the model. This meant that there were now 12 parameters to be optimised so initial guesses from Gamry were used. The curvefit method provided excellent fits to the data across all DC biases. An example fit is shown on figure 15 for 0.5 V as the other voltages provide similar fits so were omitted to avoid repetition. The Python code appears to find superior optimised parameters for the model than Gamry, demonstrated by the closer fit to the data points. However, a closer fit may not give physiological suitable parameters.

Table III shows the optimised values for the parameters associated with the potassium (*kch*) channel. Some of the resistances shown are negative. Negative resistance may raise concern as it is not physical however negative differential resistance (NDR) is one of the features associated with the impedance loop at low frequencies that causes spiking behaviour. NDR is a feature whereby current increases as voltage decreases across a component, paralleling the case with charge and voltage in negative capacitance. Therefore, it may not be as outlandish an idea as it seems to accept the negative resistance as a valid fit parameter rather than a mistake. Perhaps a future direction for the project would be further research into the physiological difference between negative resistance, negative capacitance and inductance. Negative resistance is characteristic of sodium ion channels[10] so perhaps the presence of negative resistances in the resistor of the generalised ion channel branch is very much physical and representative of the fact that *E. coli* have sodium ion channels. Negative resistance is seen in both the wildtype and mutant strain which makes sense as removing the potassium channel should not affect presence of a sodium channel.

When investigating the emergent negative resistance, we put constraints on our fit such that all resistors could only take positive values. This was done by applying bounds on the curvefit function. This made our fits much more similiar to Gamry, so the fits produced with only positive resistances were not as close fitting to the data points. It was an interesting discovery and something to consider when using Gamry that perhaps Gamry fits are constrained not to allow negative resistances. The choice between methods depends on the nature of the data. Perhaps in some cases a worse fit with non negative resistors is preferable but in this case it seems that a negative resistance is no less physical than a negative capacitance so is acceptable. The resistor that is negative is modelling a variable resistor and battery for small perturbations and the variable resistor and battery are modelling the behaviour of an ion channel. The resistor therefore doesn't have a direct physiological equivalent so may be permitted to be negative.

The parameters relating to the potassium ion channel obtained from these fits are summarised in table III with comparisons to the values stated in Akabuogu's article. There is significant deviation from Akabuogu's values in the Python fit. The deviation in R_{kch} is not worrying as the three resistors in their own branches give the model three parameters to optimise where one resistor could equally have described their action. This means resistance of one parameter can be higher or lower and made up for in the others but give a very similar overall fit.

When interpreting the results for parameter values, it must be appreciated that the code is unable to differentiate between R_q, R_{kch} and R_l. This is clear from looking at the impedance equations used. We are assigning a different physiological

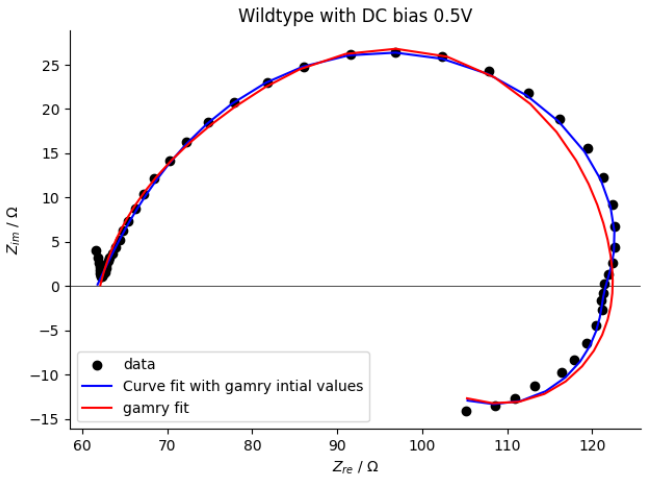

FIG. 15. A Nyquist plot for wildtype *E. coli* showing the data points in black, the Gamry fit in red and our Python fit in blue.

meaning to each resistor that is not specified in the code. Essentially, the values obtained from the fit for R_q, R_{kch} and R_l are interchangeable. The high uncertainty values on R_{kch} and R_q are therefore to be expected and the values for R_l are not listed but can be reproduced from the code in the supplementary information.

The values for membrane capacitance C_m produced by the fits were: 1.5 ± 0.2, 1.6 ± 0.2 and 1.1 ± 0.1 all in μF for 0.4, 0.5 and 0.6 bias voltages respectively. The membrane capacitance was the least sensitive parameter to the fits, which is reflected in the smaller uncertainties. Assuming the biofilm coated the whole surface of the working electrode which was 4 cm^2 the specific membrane capacitances would be would be 0.37 ± 0.05, 0.40 ± 0.01 and 0.25 ± 0.05 μFcm^{-2}. The specific membrane capacitance for a neuron stated by Golowasch[20] was 0.5 μFcm^{-2}. The values we obtain for the biofilm are not within the neuronal range with uncertainties taken into account. The C_m values obtained would suggest that bacterial biofilms may have specific membrane capacitance on the same order of magnitude as neurons. To explore this further, more accurate data would need to be collected on the area of the biofilm.

Finally, we are modelling biofilms using models which are for one neuronal cell but the biofilms consist of extremely high numbers of cells. We are therefore comparing one ion channel of a neuron to a network of many ion channels in a biofilm so perhaps parameter values would be more valid if we were to model the action of each cell in the biofilm, rather than treat it as a whole. Perhaps modelling the biofilm as a neuronal network would be more effective and could be an interesting future direction of the project.

TABLE II. This table shows the fit parameters for the generalised ion channel branch of circuit c for DH5α.

DC bias / V	R_q/Ω	R_n/Ω	L_n/H	τ_n/s
0.4	$80 \pm 10 \times 10^6$	-18 ± 2	2 ± 2	-0.1 ± 0.1
0.5	$70 \pm 20 \times 10^6$	-8 ± 1	2 ± 3	-0.3 ± 0.4
0.6	$107 \pm 40 \times 10^6$	800 ± 400	-30 ± 30	-0.04 ± 0.04

IX. PSEUDEMONAS

We also fit EIS data from *P. aeruginosa* using the Hodgkin-Huxley model for 2 ion channels (or, more specifically, one ion channel and one channel representing the collective action of all other ion channels). We used the same method and equations as for the *E. coli* wildtype because the *P. aeruginosa* being studied had not been mutated to remove ion channels. This yielded good fits, shown in figure 16.

The values for membrane capacitance extracted from the fits were $(5 \pm 9) \times 10^{-5}$, $(9 \pm 3) \times 10^{-4}$ and $(5 \pm 1) \times 10^{-4}$ F for DC biases of 1.5, 1.7 and 1.9 V. These have higher uncertainties and greater range than for *E. coli*. The greater range could be explained by the fact that the membrane capacitances for *P. aeruginosa* are taken over a larger range of DC biases. The generally higher values seen for *P. aeruginosa* could suggest that *P. aeruginosa* has higher membrane capacitance than *E. coli*. To be sure this is the case, rather than the influence of a higher bias voltage, it would be necessary to compare the capacitances at the same dc voltages.

The optimised values for components relating to electrode effects are summarised in table IV. ϕ takes a value between 0 and 1 which is as expected, signifying the model is working correctly. T is associated with the double layer capacitance and interestingly all values have the same order of magnitude as the membrane capacitance at that voltage. This would imply the double layer capacitance of the electrode is similar to the membrane capacitance which is unexpected. R_{sol} has fairly small percentage uncertainties across all bias voltages indicating that the model is highly sensitive to it. The range is around 7 Ω which is very small compared to the range of other resistors.

The resistance values R_q, R_{kch} and R_l are not shown, as the values are somewhat arbitrary, so drawing physiological conclusions would be unsubstantiated, as previously discussed. Their values have a range of around 700 Ω and uncertainties of order 10^5. The large uncertainties are a reflection of the redundancy of the parameters.

The fit parameters for the inductor resistor branches are summarised in tables V and VI. Negative values are always seen in the time constant ($\tau_i = \frac{L_i}{R_i}$) of at least one ion channel. This could perhaps reflect that the presence of sodium ion channels in *P. aeruginosa* is related to the negative induc-

TABLE III. This table shows the fit parameters for the parameters related to the potassium branch for DH5α.

DC bias/ V		R_{kch}/Ω	R_m/Ω	L_m/H	τ_m/s
0.4	Akabuogu	140 ± 1	(6 ± 3) $\times 10^{-7}$	53.8 ± 0.1	(10 ± 5) $\times 10^{-7}$
	Python	86 ± 20 $\times 10^{6}$	8 ± 3	50 ± 6	0.16 ± 0.06
0.5	Akabuogu	181 ± 1	125.4 ± 0.8	0.94 ± 0.01	(750 ± 9) $\times 10^{-5}$
	Python	68 ± 20 $\times 10^{7}$	1.8 ± 0.6	30 ± 20	0.07 ± 0.06
0.6	Akabuogu	211 ± 3	220 ± 1	2.68 ± 0.02	(121 ± 1)$\times 10^{-4}$
	Python	60 ±10 $\times 10^{6}$	18 ± 5	20 ± 10	0.7± 0.4

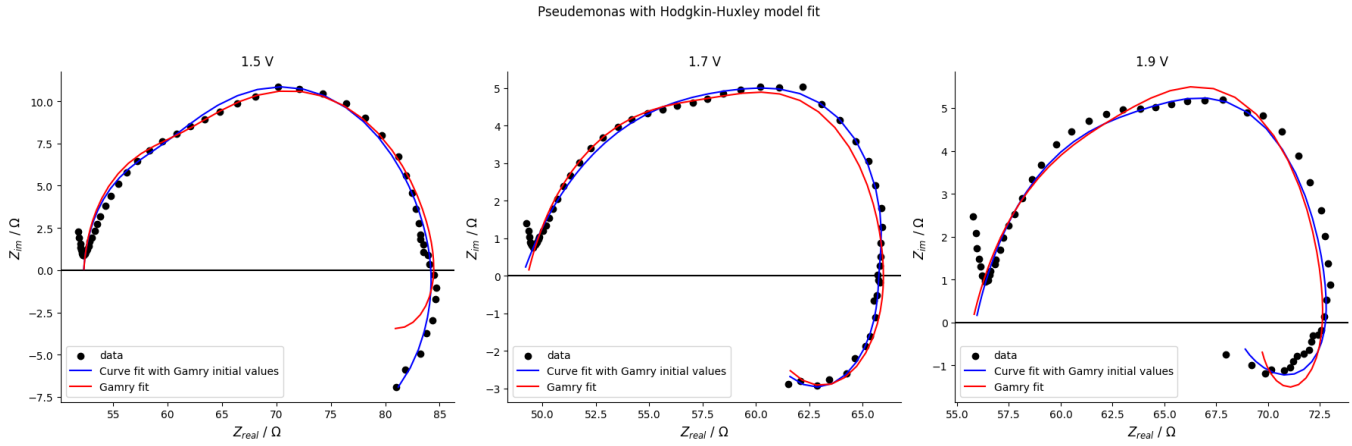

FIG. 16. A Nyquist plot for wildtype *P. aeruginosa* showing the data points in black, the Gamry fit in red and our Python fit in blue.

TABLE IV. The fit parameters for the CPE component of pseudemonas.

DC bias / V	R_{sol}/Ω	R_{ct}/Ω	T /Fcm^{-2}	ϕ
1.5	52.3 ± 0.2	26.6 ± 0.9	(32 ± 2)$\times 10^{-5}$	0.84 ± 0.02
1.7	49.07 ± 0.09	14 ± 1	(5 ± 1)$\times 10^{-5}$	0.65 ± 0.02
1.9	55.9 ± 0.2	11 ± 2	(3± 1)$\times 10^{-5}$	0.74 ± 0.05

TABLE V. This table shows the fit parameters associated with the *n* ion channel.

DC bias/ V	R_n/ Ω	L_n/ H	τ_n /s
1.5	-4.0 ± 0.4	3.1 ± 0.9	-0.8 ± 0.2
1.7	11 ± 8	0.2 ± 0.5	0.02 ± 0.02
1.9	10 ± 13	-5 ± 4	-0.4 ± -0.6

tance loop at low frequencies. To draw firm conclusions, the model would have to be fit to *P. aeruginosa* with different fitting routines and variations to see if the parameter values are a function of the specific fit or the data.

TABLE VI. This table shows the fit parameters associated with the *m* ion channel.

DC bias/ V	R_m/ Ω	L_m/ H	τ_m /s
1.5	6.5 ± 600	-9 $\times 10^{-5}$ ± 0.01	-1$\times 10^{-5}$ ± 0.001
1.7	-1.56 ± 0.04	0.7 ± 0.6	-0.5 ± 0.2
1.9	3 ± 3	2 ± 1	0.7± 0.9

X. CONCLUSION

We have presented a method to fit EIS data from wildtype and knock down mutant biofilms. This was done on Python utilising the curvefit function as it was found to be a more robust fitting procedure than NM or GD. The code improves on values from Gamry software when using Gamry initial parameters and can model the low frequency inductive loop where Gamry fails to do so. Quantifying the goodness of fit could be a worthwhile feature to add to our code. We found that Gamry software returns different optimised parameters, depending on the wiring used, even when the circuits are equivalent. Furthermore, we found that Gamry constrains resistor values to positive, so does not consider negative resistance when optimising fits. The Hodgkin-Huxley model with the addition of a Randles circuit with a CPE element best modelled the biofilms

for the wildtype and mutant *E.coli*. The Hodgkin-Huxley model for the wildtype contained extra branches to represent the action of the *kch* channel. Negative resistances were obtained in the mutant and generalised ion channel branch of the wildtype. No negative resistance values were found for the *kch* channel, perhaps confirming that it is not a sodium channel and the model successfully represents the existence of individual ion channels within the wildtype. To study whether the negative resistance is related to the sodium channel, the fits could be carried out on data from an *E.coli* knock down mutant with the sodium channel removed. The resistances showed variability and uncertainties larger than the values, indicating that the model is over-parameterised. Our code was extended to *P. aeruginosa*. It could be used to study the ion channels of other bacteria such as *Bacillus subtilis*, or even perhaps viruses. To summarize, a code has been developed that provides successful fits but because the models are physiologically derived, they contain redundant parameters. This means there can be many equivalent fits with different parameters so conclusions about the electrophysiology of the biofilm must be drawn from the less sensitive parameters. To extend the project, sensitivity analysis of the parameters would be a beneficial addition to the code.

[1] A. Prindle, J. Liu, M. Asally, S. Ly, J. Garcia-Ojalvo, and G. M. Süel, "Ion channels enable electrical communication in bacterial communities," Nature **527**, 59–63 (2015).

[2] R. S. L. L. N. Lene K. Vestby, Torstein Grønseth, "Bacterial biofilm and its role in the pathogenesis of disease," Antibiotics (Basel) **9(2)**, 59 (2020).

[3] J. W. Costerton, "Microbial biofilms," Annual Review of Microbiology **49**, 711–745 (1995).

[4] H. Benzian, "Global health threats are also oral health threats," Elsevier - PMC COVID-19 Collection **154(5)**, 367–369 (2023).

[5] C. Potera, "Forging a link between biofilms and disease," Science **154(5)**, 1837–1839 (1999).

[6] G. Sharma, "Escherichia coli biofilm: development and therapeutic strategies," Journal of applied Microbiology **121(2)**, 309–19 (2016).

[7] B. H. Iglewski, *Medical Microbiology. 4th edition* (University of Texas Medical Branch at Galveston, 1996) Chap. 27.

[8] H. S. Magar, "Electrochemical impedance spectroscopy (eis): Principles, construction, and biosensing applications," Sensors (Basel) **21(19)**, 6578 (2021).

[9] A. C. lazanos, "Electrochemical impedance spectroscopy- atutorial," American Chemical Society **3**, 162–193 (2023).

[10] Bou, Agustín, and J. Bisquert, "Impedance spectroscopy dynamics of biological neural elements: From memristors to neurons and synapses," The Journal of Physical Chemistry B **125**, 9934–9949 (2021).

[11] A. K. Jonscher, "The physical origin of negative capacitance," Journal of the Chemical society, Faraday transactions 2: Molecular and Chemical Physics **82**, 75–81 (1986).

[12] K. S. Cole, *Membranes, Ions and Impulses* (University of California Press, Berkeley, 2023).

[13] D. Klotz, "Negative capacitance or inductive loop? – a general assessment of a common low frequency impedance feature," Electrochemistry Communications **98**, 58–62 (2019).

[14] E. U. Akabuogu, L. Zhang, R. Krašovec, I. S. Roberts, and T. A. Waigh, "Electrical impedance spectroscopy with bacterial biofilms: neuronal-like behaviour," (2023), https://doi.org/10.1101/2023.11.24.568527.

[15] M. F. Sheets, "Methods in neurosciences," Electrochemistry Communications **19**, 169–188 (1994).

[16] K. S. Cole, *Membranes, Ions and Impulses* (University of California Press, Berkeley, 2023) p. 77.

[17] A. Hodgkin and A. Huxley, "A quantitative description of membrane current and its application conduction and excitation in nerve," The Journal of physiology **117(4)**, 500–44 (1952).

[18] G. H. Rutherford, "Analog implementation of a hodgkin–huxley model neuron," American Journal of Physics **88**, 918–923 (2020).

[19] W. Gerstner, W. M. Kistler, R. Naud, and L. Paninski, *Neuronal Dynamics* (Cambridge University Press, 2014).

[20] J. Golowasch and F. Nadim, "Capacitance, membrane," in *Encyclopedia of Computational Neuroscience*, edited by D. Jaeger and R. Jung (Springer New York, New York, NY, 2013) pp. 1–5.

[21] E. L. R. Compton and J. A. Mindell, "Bacterial ion channels," EcoSal Plus **1** (2010).

[22] J. W. Karpen, "Ion channel structure and the promise of bacteria : Cyclic nucleotide-gated channels in the queue," Journal of General Physiology **124**, 199–201 (2004).

[23] R. Iyer, T. Iverson, A. Accardi, and C. Miller, "A biological role for prokaryotic clc chloride channels," Nature **419(6908)**, 715–8 (2002).

[24] N. Ford and A. prindle, "A two-dimensional model of potassium signaling and oscillatory growth in a biofilm," Bulletin of Mathematical Biology **Volume 83** (2021).

[25] S. Ruder, "An overview of gradient descent optimization algorithms," arXiv:1609.04747v2 (2017).

[26] H. P. Gavin, "The levenberg-marquardt algorithm for nonlinear least squares curve-fitting problems," Department of Civil and Environmental Engineering Duke University (2022).

[27] *Curvefit Documentation*, The SciPy community, API reference, scipy v1.11.4 manual ed.

[28] J. A. Nelder and R. Mead, "A simplex method for function minimization," The Computer Journal **7**, 308–313 (1965).

[29] J. H. Mathews and K. K. Fink, *Numerical Methods using Matlab*, 4th ed. (Prentice-Hall Inc., 2004).

[30] B. Efron, "Bootstrap methods: Another look at the jackknife," The Annals of Statistics **7**, 1–26 (1979).

[31] R. Andrae, T. Schulze-Hartung, and P. Melchior, "Dos and don'ts of reduced chi-squared," arXiv:1012.3754v1 (2010).

[32] L. Chua, "Memristor-the missing circuit element," IEEE Transactions on Circuit Theory **18**, 507–519 (1971).

[33] *Basics of Electrochemical Impedance Spectroscopy*, Gamry Instruments, 734 Louis Drive, Warminster, PA 18974, United States of America, april 17, 2021 ed., an application note.

[34] J. Wu, "Understanding the electric double-layer structure, capacitance,and charging dynamics," Chemical Reviews **122 (12)**, 10821–10859 (2022,).

[35] P. Biesheuvel, "The difference between faradaic and non-faradaic electrode processes," arXiv:1809.02930v4 (2021).

[36] S. Mohammad, R. Niya, and M. Hoorfar, "On a possible physical origin of the constant phase element," Electrochimica Acta **188** (2016).

[37] andrzej Lasia, "The origin of the constant phase element," American Chemical Society **13**, 580–589 (2022).

[38] S. M. Gateman, "On the use of a constant phase element (cpe) in electrochemistry," Current Opinion in Electrochemistry **36** (2022).

[39] L. Nyikos and T. Pajkossy, "Fractal dimension and fractional power frequency-dependent impedance of blocking electrodes," Electrochimica Acta **30,11** (1985).

[40] B. Boukamp, English"A linear kronig-kramers transform test for immittance data validation," Journal of the Electrochemical Society **142**, 1885–1894 (1995).

[41] K. S. Cole, *Membranes, Ions and Impulses* (University of California Press, Berkeley, 2023) p. 55.

[42] A. O. Alvarez, R. Arcas, C. A. Aranda, L. Bethencourt, E. Mas-Marzá, M. Saliba, and F. Fabregat-Santiago, "Negative capacitance and inverted hysteresis: Matching features in perovskite solar cells," The Journal of Physical Chemistry Letters **11**, 8417–8423 (2020), pMID: 32903005.